

Microstructural analysis of lignocellulosic fiber networks

T. Walther^a, K. Terzic^b, T. Donath^c, H. Meine^b, F. Beckmann^c, H. Thoemen^a

^aUniversity of Hamburg, Department of Wood Science,
Leuschnerstrasse 91, 21031 Hamburg, Germany

^bUniversity of Hamburg, Department of Informatics,
Vogt-Koelln-Strasse 30, 22527 Hamburg, Germany

^cInstitute for Materials Research, GKSS-Research Center,
Max-Planck-Straße 1, 21502 Geesthacht, Germany

ABSTRACT

The structure of wood based medium density fiberboard (MDF) has been studied using synchrotron radiation-based x-ray microtomography (SR μ CT.) Fully automated 3D segmentation and analysis routines have been developed in order to gain information about individual fibers, the distribution of the fiber material, fiber orientation, fiber surfaces and size and location of contact areas. Representative samples of the analyzed volume data are presented to demonstrate the results of the implemented methods using the VIGRA image processing library.

Keywords: image analysis, medium density fiberboard, microtomography, segmentation, synchrotron radiation, VIGRA, wood fibers, x-ray tomography

1. INTRODUCTION

The use of lignocellulosic fibers from wood and annual plants for the production of fiber composites has gained high importance during the last years. Many applications in the furniture industry, for laminate flooring and for automotive purposes show that the production of these composites requires comprehensive knowledge about its structure to improve production quality and performance under service conditions.

The investigation on the microstructure by light and electron microscopy is difficult due to surface artifacts caused by the high sensitivity of the samples towards mechanical treatment during sample preparation. A promising approach is the use of microtomography as a powerful tool to investigate the unchanged 3D-structure of materials. Microtomography allows virtual cuts through the sample in any direction and it supplements classical microscopy research techniques. The qualitative and quantitative analysis of microtomography images using 3D image analysis offers a wide variety of methods that can be used to discover the undamaged interior parts of the samples. This analysis has to be adjusted to fit the requirements of the material structure.

In this study, the microstructure of medium density fiberboards (MDF) has been investigated using synchrotron radiation-based X-ray microtomography (SR μ CT) at beamline BW2 of the Hamburger Synchrotronstrahlungslabor (HASYLAB) at the Deutsches Elektronen-Synchrotron (DESY) in Hamburg, Germany. The methods developed to investigate and analyse the tomographic data by using 3D algorithms will be explained. Previous research on fiberboard structures using microtomography^{1,2} mainly focused on simulating the structure and only little information is available about the quantitative and qualitative analysis of the structure itself.^{3,4}

The structure of MDF is strongly dependent on the physical and chemical mechanisms that occur during the hot-pressing process. In this process, the loosely formed mat of adhesive-treated wood fibers is consolidated under severe conditions with high pressures and temperatures of 200°C and above. Important mechanisms during consolidation are heat and mass transfer through the porous wood fiber mat, the densification and stress relaxation process of the fibers, and adhesive cure. A few approaches to model the complex hot-pressing process

Contact via: terzic@informatik.uni-hamburg.de; phone +49 40 42883-2580; fax +49 40 42883-2572; kogs-www.informatik.uni-hamburg.de

have been presented in the last years.⁵⁻⁷ Nevertheless, examinations of the microstructure of wood composite materials are necessary for a realistic modeling and to understand the relation between the microstructural features and the mechanical behavior of the end product.

2. INSTRUMENTS

2.1. Sample preparation

Different MDF samples made of commercial fiberboard furnish consisting of softwood fibers (*Pinus sylvestris*) have been prepared. The fibers were treated with an urea formaldehyde adhesive (UF-resin) in a drum blender resulting in a total resin content of 10% solid resin related to the dry weight of the board.

Laboratory MDF boards with a thickness of 5 mm and a diameter of 100 mm with target densities ranging from 300 kg/m³ to 1000 kg/m³ were produced using a computer-controlled miniature hot-pressing system simulating industrial manufacturing of fiberboards. By using a standardized pressing program a symmetrical vertical density profile in the boards with maximum densification in the surface layers and a minimum densification in the middle layer was built up during hot-pressing.

2.2. Microtomography

For the microtomographic investigation, a sample of about 2 × 2 mm size was cut out from each 5 mm thick fiberboard, thus, resulting in samples with a volume of about 2 × 2 × 5 mm. Only one half of the samples had to be investigated because of the symmetrical density profile of the boards.

All samples were surveyed with SRμCT at the BW2 beamline of the HASYLAB, DESY. The measurements were carried out using the microtomography apparatus operated by GKSS in January 2005. Optimized conditions for tomography could be achieved by adjusting the photon energy and the magnification of the X-ray camera. With the double-crystal monochromator (Si-111) of beamline BW2, a photon spectrum centered at $E = 12$ keV photon energy and with small bandwidth ($\Delta E/E \approx 10^{-4}$) was selected. The current setup of the X-ray camera was described elsewhere;⁸ basically, it consists of a CdWO₄ scintillation crystal lens-coupled to a CCD camera with a pixel size of $\tau_0 = 9 \mu\text{m}$. Translation of the optical components was used to select the optical magnification factor m , which in this case was set to $m = 3.94$ resulting in an effective pixel size of $\tau_0/m = 2.28 \mu\text{m}$. The spatial resolution (corresponding to 10% contrast transfer) was determined from the measurement of an edge profile as 3.90 μm . The CCD size of 1536 × 1024 pixels thus corresponds to a field-of-view of 3.51 × 2.34 mm², which was entirely covered by the X-ray beam.

For each scan, 720 projections were recorded with the full CCD size of 1536 × 1024 pixels at projection angles between 0° and 180° in steps of 0.25°. Reference images required for normalization were recorded typically every eight projections as well as before and after the scan. The projection data was reconstructed as a stack of 2D reconstructions using the BKFIL filtered-backprojection algorithm of the `rec1b1` library⁹ on a 1536 × 1536 pixel grid, resulting in a total reconstructed volume of 1024 × 1536 × 1536 voxels per scan, stored as single precision floating-point values. Two overlapping scans were recorded and subsequently combined such that more than half of the sample thickness was covered.

2.3. 3D image analysis tools

In order to reduce the computational costs and make 3D image analysis feasible, 30 sub-volumes with a size of 256 × 256 × 256 voxels and 27 sub-volumes with a size of 512 × 512 × 256 voxels were extracted from the 3D data sets. This also supports local characterization of the fiber packaging and prevents problems with surface effects. For every scan, several sub-volumes with varying distance from the sample surface were analysed. Furthermore, the interesting value range from the floating point reconstructions has been selected and reduced to an 8-bit representation.

The resulting sub volumes were analysed using methods described in detail in the next section. The employed image processing algorithms have been implemented in the context of the open-source VIGRA image processing library,¹⁰ developed at the Cognitive Systems Laboratory (CSL), University of Hamburg. The VIGRA library has a toolbox-like architecture, providing (n-dimensional) image data structures and optimized implementations

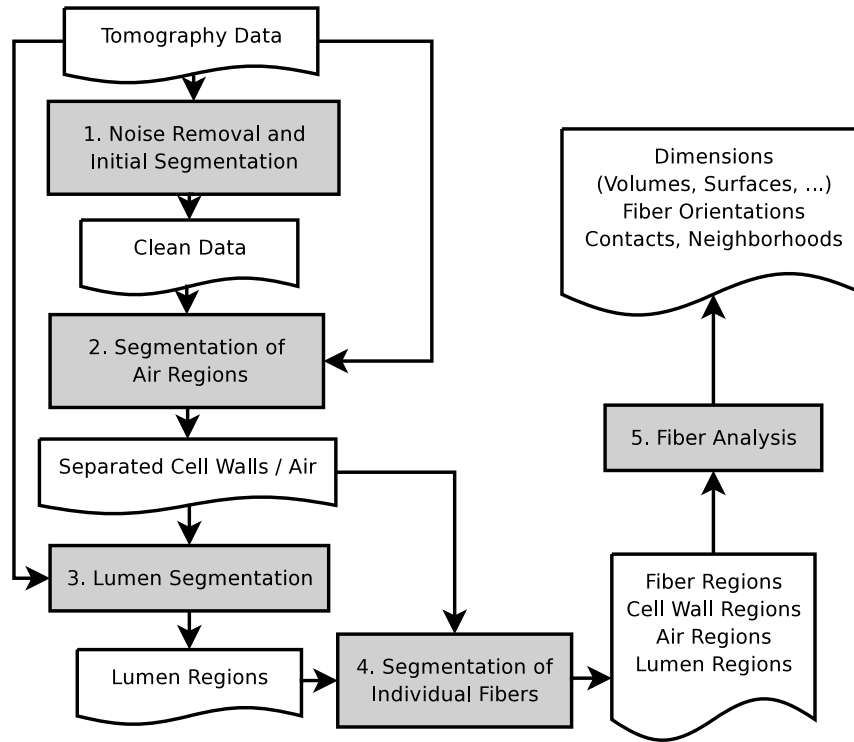


Figure 1. Flow chart for segmentation and image analysis of the selected sub volumes from the original tomography data.

for many standard image processing algorithms. Its focus on generic programming makes it possible to retain efficiency while offering a great flexibility through small, combinable building blocks.

Visualizations were performed using the VIGRACaster, an interactive 3D visualization tool based on VIGRA (also developed at the CSL.) All algorithms developed for the MDF data were implemented in C++ using VIGRA.

3. METHODS

The segmentation steps and the image analysis of the sub volumes are shown in the flow chart in Figure 1. The following subsections will explain the five depicted main analysis steps in detail.

3.1. Noise removal and initial segmentation

The segmentation of tomography data is complicated by noise and systematic errors in the reconstructions. While noise is uncorrelated and can be dealt with, the systematic errors, which are most probably caused by the limited number of sampling points and blur in the detector system, impose a problem. They reach up to 30% of the maximum cell wall density in regions which should contain nothing but air. It is also dense enough to result in connected regions of high-intensity voxels after 3D thresholding, forming complex fractal-like structures. Such regions are often close to cell walls, and even enclose low-intensity regions, resulting in lumen-like configurations. Thus, removal of the systematic errors proved to be the most difficult part of segmenting the 3D volumes.

Due to the voxel edge length of $2.3 \mu\text{m}$, a typical fiber wall is only one or two voxels thick. Thus, simple morphological operations damage too many fibers and prevent further segmentation. Our approach is based on the assumption that all fibers have to be physically connected in order to form a solid material, whereas noise appears randomly throughout the image. Fibers also form more salient regions, compared to the erratic structure of noise.



Figure 2. Result of the noise removal stage shown on a representative slice. *Left:* Original data with marked ROI. *Middle:* Thresholding process; cell wall voxels $\geq t_{\text{high}}$ (dark gray), additional neighbored voxels $\geq t_{\text{low}}$ (black), small regions of noise voxels $\geq t_{\text{high}}$ (light gray.) The light red regions inside the fiber walls represent the fiber lumen. *Right:* Data after noise removal.

In order to suppress the noise, we first apply an aggressive threshold, resulting in a binary volume selecting voxels with high value $\geq t_{\text{high}}$ only (high values in the tomographic images correspond to high material density.) The size of each connected component of marked voxels is determined, and only the largest region is selected as fiber material since all fibers are meant to form one connected component. All other small, singular regions surrounded by air are assumed to be a result of noise agglomerations, and they are therefore removed from the volume.

3.2. Segmentation of air regions

The remaining binary volume now contains a large region that represents the cell wall material. This first segmentation into cell wall and air regions is not yet accurate because it does not include all fiber material due to the high threshold used against the noise. Because of this, a second, lower threshold t_{low} is used afterwards, but only in the vicinity of the voxels which were above the first threshold. This approach restores many of the cell wall voxels with low intensity. It is implemented by dilating (growing) the region of the previous step by $\sim 3.5 \mu\text{m}$ (one voxel.) and used as a mask for the new thresholding operation. It should be noted that all morphological operators used at this scale (one voxel) are anisotropic, exhibiting different effects in different directions, so the operator radius is an approximation. The result is a successful binary segmentation into cell wall and air voxels (Figure 3 left.)

The actual values of the two thresholds depend on the exact parameters used when making the 3D images (e.g. beam intensity), the resolution of the volumes (at lower resolutions many voxels will be only partially covered by material, resulting in a lower intensity) and the noise levels in the volume. In our case, the relation of both thresholds was $t_{\text{high}}/t_{\text{low}} = 3$. The results of the noise removal with these settings are shown in Figure 2.

3.3. Lumen segmentation

The intensity-based segmentation used so far cannot distinguish between air enclosed inside a fiber, the so-called lumen, and the air between fibers that is accessible from outside. To locate voxels representing lumen, each air region has to be analysed separately, and those regions which are enclosed within cell wall voxels have to be marked. Another characterizing property of these regions is their thin, elongated shape. Outside air, on the other hand, forms very large regions around the fiber cell walls.

Tiny holes in the fiber cell walls, which occur both naturally and as a result of fiber damage during processing, were found to make this region-based approach difficult. Many lumens are connected to outside air through such small holes, so that a simple connected component analysis combines them with the outside air into one large region. In order to prevent this, we close the holes by using morphological operators.

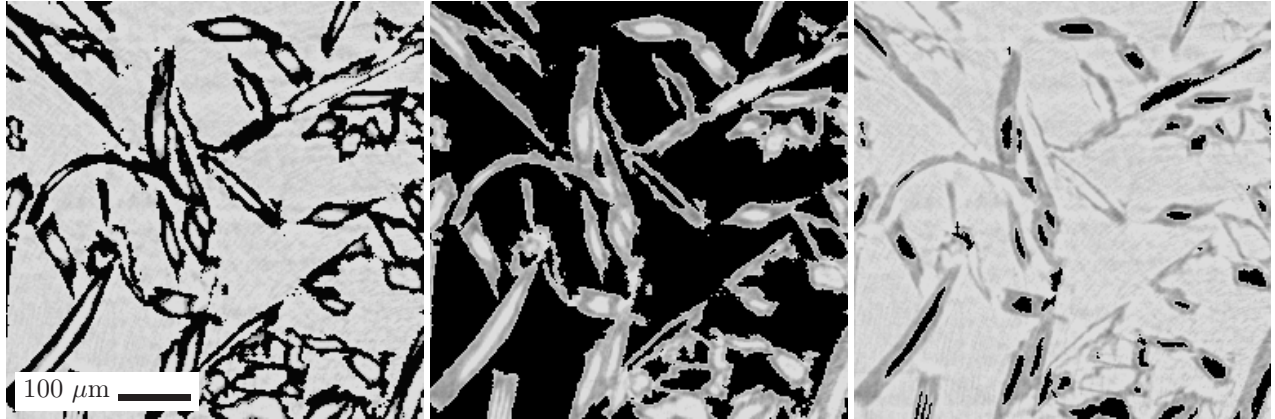


Figure 3. Representative slice of a sub-volume (256×256 pixels) with a density of 300 kg/m^3 after segmentation. Segmented regions in black (background for orientation purposes): *Left:* Cell walls. *Middle:* Outside air. *Right:* Lumen.

First, a binary erosion operator is applied to the air region, effectively closing all holes smaller than the structuring element, which was a sphere with $r \approx 3.5 \mu\text{m}$ (one voxel.) Then, a 3D Euclidean distance transformation is applied on each connected component of air voxels, determining the maximum radius of an inscribed sphere for each region, which is a measure of thickness. Since lumen regions are thin and elongated, they cannot contain large spheres, while air regions between fibers locally have higher distance values. All air regions where all distance values are below $\sim 10 \mu\text{m}$ (4.5 voxel) are classified as lumen regions, the remaining regions are classified as outside air.

Since the *erosion* operator used above effectively shrunk the air regions, we recover their exact original boundaries by (a) *dilating* the regions with a structuring element of twice the radius as used for the erosion and (b) using the result as a mask on the original air image from the previous step (see Figure 2.)

Some of the small air regions are obviously too small to be normal lumens, and often they can be identified as small air bubbles enclosed in the adhesive resin. For this reason, all regions with a volume of $\leq 1 \text{ mm}^3$ were discarded. The remaining air regions represent the lumens inside the fibers, and we assign individual labels to each lumen. The segmented lumens can be seen in Figure 2 (middle.)

The result so far is a complete segmentation into voxels belonging to outside air, cell walls, and individually labeled lumens. Figure 3 shows three binary slices of the segmented data.

3.4. Segmentation of individual fibers

In nature, each wood fiber has exactly one lumen associated with it. Having found the individual lumens as described above, it is possible to identify individual fibers by associating cell wall voxels with the nearest lumen.

Starting with the volume containing labeled lumens, each non-lumen voxel is given the label of the nearest lumen using a combination of a Euclidean distance transform and *Seeded Region Growing*. The resulting volume is known as a *Voronoi Diagram* and separates the volume into regions of influence, with each region being associated with its nearest lumen. Then, the Voronoi diagram is masked using the previously segmented cell wall voxels, resulting in a volume with individually labeled fibers carrying the same label as their corresponding lumens. Figure 4(middle) shows a selection of individually segmented fibers. Figure 5 shows two complete sub-volumes where each identified fiber was marked with a different color.

The segmentation was found to miss some lumens because of openings in the fiber cell walls, noise artifacts, and fiber fragments in the raw material for producing the boards. The process described so far would find cell wall material and incorrectly assign it to the nearest lumen, so we determined a maximum fiber thickness and limited the distance between the cell wall voxels and the lumen they are associated with (effectively limiting the influence regions.) A maximum thickness of $\sim 14 \mu\text{m}$ (6 voxels) was found to be the optimum value for this operation. Although the fiber walls are not that thick on average, the pressing process often causes deformations at fiber contact points, especially in denser boards, resulting in large cell wall regions.

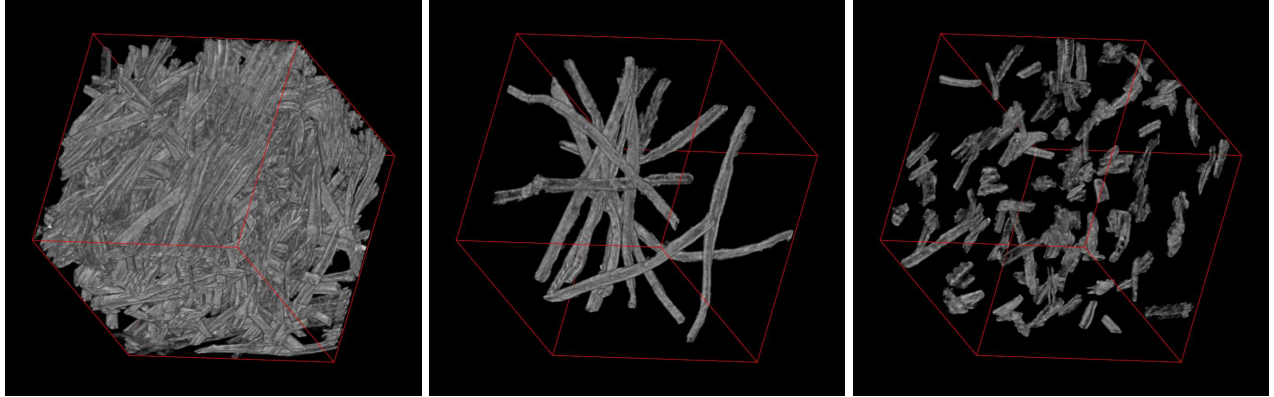


Figure 4. 3D renderings of an MDF sub-volume with a size of 256^3 voxels and a density of 300 kg/m^3 . *Left:* the complete volume; *Middle:* a selection of individually labeled fibers; *Right:* a selection of individually labeled fiber fragments with volume ≤ 1000 voxels. The side length of the displayed cube is $588 \text{ }\mu\text{m}$.

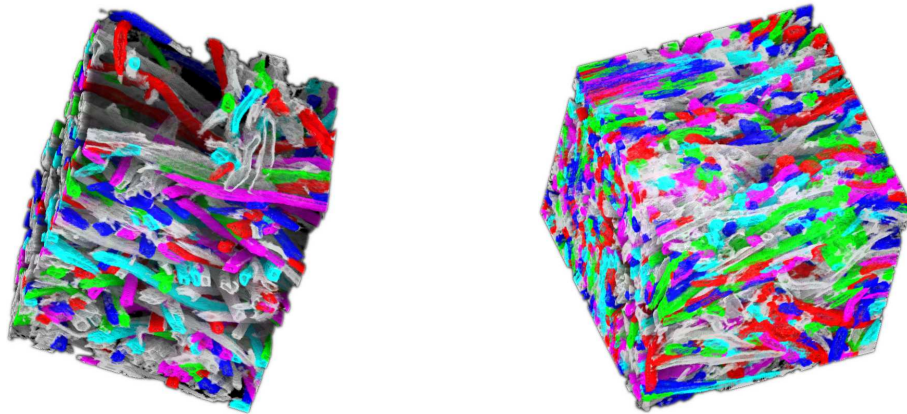


Figure 5. A sub-volume (256^3) with individually segmented fibers. The individual fibers are assigned random colors. *Left:* density of 300 kg/m^3 , *Right:* density of 500 kg/m^3 .

3.5. Fiber analysis

So far, we have a partitioning of the original 3D data into outside air, individual fibers and lumens, and fragment material, allowing for a detailed analysis of the individual parts. We are interested in the examination of fiber orientation, volumes and surface of the fibers, and the recognition of fiber bundles.

3.5.1. Fiber orientation

The orientation of the individual fibers can be calculated by performing principal component analysis. To do so, the coordinates of all voxels belonging to a given lumen are collected and the principal components of this set were determined from their covariance matrix. The Eigenvector belonging to the largest Eigenvalue represents the main direction of a lumen, and we use the angle between this Eigenvector and the original axes of the volume as lumen orientation.

3.5.2. Volume and surface

The volume of the cell wall material, outside air and lumens can be determined by simply counting the voxels belonging to each of the three classes, see Figure 6. A complete separation between outer air and lumen tends to be inaccurate for sub-volumes with a density above 1200 kg/m^3 due to a complete densification of the fibers, resulting in a collapse of the cell wall and a vanishing of the lumen. (A natural upper bound for completely densified wood fiber material would be 1500 kg/m^3 which is equal to the density of the fiber cell wall.)

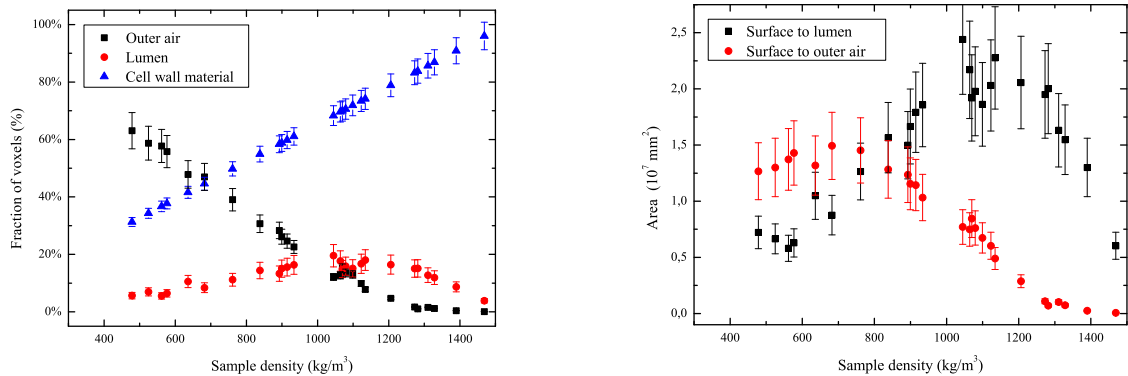


Figure 6. *Left:* Relative number of voxels (%) per sub-volume belonging to cell wall, cavities and outside air for MDF sample densities from 470 to 1470 kg/m³. *Right:* Absolute fiber surface (in μm^2) per sub-volume for MDF sample densities from 470 to 1470 kg/m³ in contact with outer air and cavities.

Additionally, the contact surface between the fiber walls and outside air is calculated by applying the Marching Cubes algorithm, a standard algorithm which creates triangle models approximating 3D surfaces.¹¹ Using the segmentation results, we use it to approximate the inside surface (between fibers and lumens) and outside surface (between fibers and outside air.)

3.5.3. Neighborhood graph and detection of fiber bundles

In order to analyze the relation between the fibers in the examined volume, first a neighborhood graph is constructed from the labeled fiber volume. The fibers represent the nodes in this graph, and the edges denote that the two fibers are connected. Weights associated with the edges represent the actual number of neighboring voxels between the two fibers.

This neighborhood graph can then be used to find fiber bundles by examining the contact surface between neighboring fibers. If two fibers share a large border (the threshold used for this analysis was set to $10^4 \mu\text{m}^2$), they are marked as belonging to a fiber bundle. Neighbors with a large contact surface are either added to an existing fiber bundle, or a new bundle is established. The process is repeated until no more neighbors share a common surface greater than the above value. Figure 7 illustrates some example result of this bundle recognition.

4. RESULTS AND DISCUSSION

The method used for segmenting individual fibers can only be as accurate as the lumen segmentation. Unfortunately, the noise levels and the resolution of our tomography data make this task very difficult. The main problems with fiber segmentation are false positives, oversegmentation and undersegmentation.

False positives occur where strong clusters of noise voxels directly neighbor a fiber wall. If such clusters are not filtered out during the noise removal step because they reach a too high intensity or are strongly connected to the fiber cell wall, air voxels are sometimes enclosed between this noise and neighboring fibers. These air voxels will then be mistaken for lumens or lumen fragments and result in very small lumps of enclosing cell wall material after the fiber segmentation step.

Oversegmentation occurs when a single lumen is split into several parts, because of noise, collapsed cell walls or very thin lumen parts which are closed by morphological operations, leading to a segmentation of a single fiber into several fiber fragments.

Undersegmentation appears in the case where two lumens are connected to each other, usually because of a small opening in the fiber cell wall between them, which is not closed by the lumen segmentation algorithm. In this case, several fibers will be represented by one label. This often happens with bundled fibers.

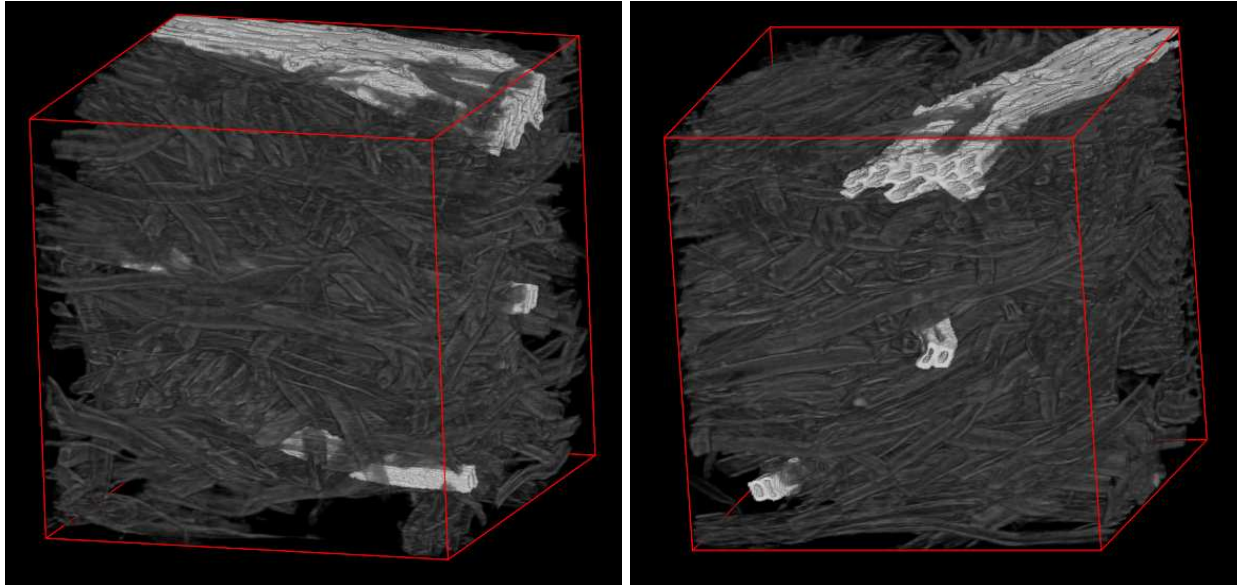


Figure 7. Automatically segmented bundles from a 256^3 sub-volume with a density of 300 kg/m^3 , shown from two different angles.

4.1. Evaluation of the results

Unfortunately, there is no *ground truth* that MDF board segmentation results can be compared to. With very thick materials (750 kg/m^3 and higher), the labeling becomes difficult even for human experts, as fibers are pressed together and some bubbles of outside air are pressed into lumen-like formations. Therefore, the evaluation of the results had to be based on 3D visual inspection (e.g. using our VignaCaster software) and the comparison of the calculated values with the results of other methods (if possible.)

The correct segmentation of fiber lumens remains a difficult problem. The openings in the cell wall are often larger than the average lumen width and are not successfully removed by the algorithm, resulting in the classification of such lumens as outside air. It is impossible to determine how many lumens were correctly segmented, but about 25% of voxels classified as cell wall material in the lighter materials were not near a recognized lumen, and as such were not labeled as individual fibers. Assuming that the probability of having such large openings is independent of the fiber size, the size distribution is the same for labeled and unlabeled fibers, and we thus estimate that 75% of the lumens are correctly classified as such. This result improves with increasing density of the material, since there is less outside air in the material and fewer openings due to the density of the material. Improved imaging techniques, signal-to-noise ratio, or increased resolution are expected to improve this result.

The visual inspection of the volumes after segmentation showed that about 20% of the labels were assigned to complete fibers, and further 70% of labels are assigned to fragments of complete fibers. This means that a single fiber is often split into several segments, with each segment having a separate label. False positives represent about 10% of all fiber labels. The false positives are very small, however, and represent less than 2% of the actual cell wall material. We can only filter out some of these fragments by size, because some real fiber fragments are also quite small. Furthermore, some fibers get merged together due to undersegmentation, but they are few. Most of the time such fibers belong to larger fiber bundles, and are identified as such by the algorithm described in section 3.5.3. Our current work is geared towards merging fiber fragments into whole fibers by analyzing the neighborhood graph, the contact points, and the orientation of the fragments.

The analysis of the segmented volumes shown in Figure 6 shows a proportional increase in the cell wall material and a logarithmic decrease of the outside air volume with increasing board density, which is the expected behavior. The volume of lumen regions rises steadily due to the increased number of fibers, but levels off and starts decreasing around 1000 kg/m^3 as the lumen regions collapse due to pressure, which is also expected.

The orientations calculated for the individual fibers show a random spread of orientations in the XY plane, but a lower average inclination in the XZ and YZ planes. This result is also confirmed by the visual inspection of 3D volumes.

The segmented 256^3 subvolumes were also used for the simulation of the permeability and thermal conductivity at the Fraunhofer ITWM in Kaiserslautern, Germany. The results of the simulation were very close to experimentally determined values, providing more reassurance in the results of our method.

4.2. Comparison to similar work

There are two current approaches for automatically segmenting individual fibers in lignocellulosic materials known to us. Wiig and Henden¹² propose a method for segmentation of individual paper fibers based on lumen tracking with interactive selection of seed points. They also propose an algorithm for automatically selecting seeds and report that it finds 50-70% of all the lumens that can be tracked by their algorithm.

The resolution used in their work was as high as $0.7 \mu\text{m}$ per voxel (more than three times higher than ours in each dimension), which makes the image analysis much easier (but restricted to smaller samples).

The approach suggested by Lux et al.⁴ uses a lower resolution and performs a skeletonization of the fibers after filling in the lumens. While the skeletonization process presented in the paper is well suited for very light materials where few voxels belong to cell wall material (the boards analyzed in the paper had densities between 45 and 170 kg/m^3), its performance is expected to decrease with increasing density. At a density of about 750 kg/m^3 the volume of air is roughly the same as the volume occupied by the cell wall material, and this method is expected to break down.

The main advantages of our approach are that it can operate on a wide range of densities, does not require interaction, and that it can detect fiber bundles, which is an important problem not addressed by other approaches.

5. CONCLUSIONS

Microtomography is being increasingly used for inspecting lignocellulosic materials^{3,4,12-15} because it enables a 3D analysis of the material without damaging its structure. The automatic segmentation and evaluation of the tomography data, and especially the validation of such results, however, remain an open problem.

In this paper, an automatic segmentation method for lignocellulosic fiber structures was presented. A number of standard 3D image analysis algorithms was applied to segment the tomography data into outside air, lumen and cell walls. Additionally, individual fibers were segmented, making it possible to analyse their individual properties and automatically identify fiber bundles.

The analysis was applied on 57 different subvolumes with varying properties. Values such as the orientation of the individual fibers, the volume and surface of the air and cell wall regions, neighborhood graph, and contact surface between the fibers were calculated from the segmented volumes. The results correspond with the expected values and have already been used to observe trends related to board density.

Although some lumens are misclassified and the fiber segmentation algorithm tends to oversegment, the results are very promising, resulting in many correctly segmented fibers even in extremely dense materials (1000 kg/m^3 .) Improving the fiber segmentation through the merging of fiber fragments based on neighborhood relationships and orientation is currently being investigated. Improvements in microtomography and processing power are expected to improve the results even further.

ACKNOWLEDGMENTS

The authors gratefully acknowledge the support of the Arthur and Aenne Feindt Foundation (Hamburg) for their financial support and Volume Graphics GmbH (Heidelberg) for their technical support.

REFERENCES

1. H. Wang and S. M. Shaler, "Computer-simulated three-dimensional microstructure of wood fiber composite materials," *Journal of Pulp and Paper Science* **24**(10), pp. 314–319, 1998.
2. L. Groom, L. Mott, and S. M. Shaler, "Relationship between fiber furnish properties and the structural performance of mdf," in *Proceedings of the 33rd International Particleboard/Composite Materials Symposium*, pp. 89–100, Washington State University, (Pullman, Washington, USA), Apr. 1999.
3. M. Faessel, C. Delisée, F. Bos, and P. Castéra, "3D modelling of random cellulosic fibrous networks based on x-ray tomography and image analysis," *Composites Science and Technology* **65**(13), pp. 1931–1940, 2005.
4. J. Lux, C. Delisée, and X. Thibault, "3D characterization of wood based fibrous materials: an application," *Image Analysis and Stereology* **25**, pp. 25–35, 2006.
5. P. E. Humphrey and A. J. Bolton, "The hot pressing of dry-formed wood-based composites, part II: A simulation model for heat and moisture transfer and typical results," *Holzforschung* **43**(3), pp. 199–206, 1989.
6. B. G. Zombori, F. A. Kamke, and L. T. Watson, "Simulation of the mat forming process," *Wood and Fiber Science* **33**(4), pp. 564–579, 2001.
7. H. Thömen and P. E. Humphrey, "Modeling the continuous pressing process for wood-based composites," *Wood and Fiber Science* **35**(3), pp. 456–468, 2003.
8. T. Donath, F. Beckmann, R. Heijkants, O. Brunke, and A. Schreyer, "Characterization of polyurethane scaffolds using synchrotron radiation based computed microtomography," in *Proc. SPIE 5535*, pp. 775–782, 2004.
9. R. Huesman, G. Gullberg, W. Greenberg, and T. Budinger, "Reclbl library users manuel - donner algorithms for reconstruction tomography," Tech. Rep. PUB214, Lawrence Berkeley Laboratory, University of California, 1977.
10. U. Köthe and H. Meine, "VIGRA - vision with generic algorithms: Documentation." WWW: <http://kogs-www.informatik.uni-hamburg.de/~koethe/vigra/> [visited July, 1st 2006], Sept. 2000.
11. W. E. Lorensen and H. E. Cline, "Marching cubes: A high resolution 3D surface construction algorithm," in *Proceedings of the 14th annual conference on Computer graphics and interactive techniques*, pp. 163–169, 1987.
12. J. Bache-Wiig and P. C. Henden, "Individual fiber segmentation of three-dimensional microtomograms of paper and fiber-reinforced composite materials," Master's thesis, Norwegian University of Science and Technology, 2005.
13. R. Holmstad, O. W. Gregersen, U. Aaltosalmi, M. Kataja, A. Koponen, A. Goel, and S. Ramaswami, "Comparison of 3D structural characteristics of high and low resolution x-ray microtomographic images of paper," *Nordic Pulp and Paper Research Journal* **20**(3), pp. 283–288, 2005.
14. J. Lux, A. Ahmadi, C. Gobbe, and C. Delisee, "Macroscopic thermal properties of real fibrous materials: Volume averaging method and 3D image analysis," *International Journal of Heat and Mass Transfer* **49**(11–12), pp. 1958–1973, 2006.
15. I.-M. Sintorn, S. Svensson, M. Axelsson, and G. Borgefors, "Segmentation of individual pores in 3D paper images," *Nordic Pulp and Paper Research Journal* **20**(3), pp. 316–319, 2005.